Dalton Transactions

PAPER

View Article Online
View Journal | View Issue

Cite this: *Dalton Trans.*, 2018, **47**, 585

Solution structure of a pentachromium(II) single molecule magnet from DFT calculations, isotopic labelling and multinuclear NMR spectroscopy†

Aivaras Dirvanauskas,[a,b] Rita Galavotti,[a] Alessandro Lunghi,[c] ‡[c] Alessio Nicolini,[a] Fabrizio Roncaglia,[a] Federico Totti[c] and Andrea Cornia*[a]

Received 18th October 2017,
Accepted 4th December 2017

DOI: 10.1039/c7dt03931j

rsc.li/dalton

The structure of pentachromium(II) extended metal atom chain $[Cr_5(tpda)_4Cl_2]$ (**2**), which behaves as a single molecule magnet at low temperature, was investigated by Density Functional Theory (DFT) calculations and spectroscopic studies without the constraints of a crystal lattice (H_2tpda = N^2,N^6-bis(pyridin-2-yl)pyridine-2,6-diamine). DFT studies both in the gas phase and including CH_2Cl_2 solvent effects indicate that an unsymmetric structure (C_4 point group), with pairs of formally quadruply-bonded metal ions and one terminal metal center, is slightly more stable (2.9 and 3.9 kcal mol^{-1}) than a symmetric structure (D_4 point group). Isotopically-labelled samples (**2**-d_8 and **2**-d_{16}) have then been prepared to aid in molecular symmetry determination by combined ^{1}H and ^{2}H NMR studies in dichloromethane solution. The spectra are strongly suggestive of a symmetric (D_4) framework, indicating fast shuttling between the two unsymmetric forms over the timescale of NMR experiments. Procedures for a high-yield Pd-free synthesis of H_2tpda and for site-selective post-synthetic H/D exchange of aromatic H_2tpda hydrogens are also reported.

Introduction

One-dimensional molecular complexes containing metal–metal bonds are attractive both as simple benchmark systems for studying metal–metal interactions and as prototypical molecular wires with a prominent application potential in nanoelectronics.[1–4] Although many reported linear arrays feature unbridged metal–metal bonds,[5a] a popular synthetic strategy entails the use of properly designed bridging ligands to enforce sufficiently short metal–metal distances, so that direct overlap of d orbitals occurs.[5] A family of such complexes, known since 2003 as Extended Metal Atom Chains (EMACs),[6–9] comprise oligo-α-pyridylamines or related ligands that contain N-based heterocycles.[10] The fully-deprotonated, all-*syn* conformation of these ligands can form a helical coil and wrap around strings of up to eleven metal ions.[11,12] This ligand geometry is efficient in promoting formation of metal–metal bonds, but the exact pattern of metal–metal distances and the extent of bond delocalization have represented a much debated issue. Especially controversial is the interpretation of crystallographic data for tri- and pentachromium(II) derivatives $[Cr_3(dpa)_4Cl_2]$ (**1**) and $[Cr_5(tpda)_4Cl_2]$ (**2**) (see Scheme 1), which both behave as single molecule magnets at low temperature (Hdpa = *N*-(pyridin-2-yl)pyridin-2-amine,[13] H_2tpda = N^2,N^6-bis(pyridin-2-yl)pyridine-2,6-diamine, see Scheme 1).[14,15] The solid-state structures of these EMACs show metal atoms with abnormally elongated (prolate) displacement ellipsoids along the chain axis, which can be interpreted as due to either large thermal vibrations or to positional disorder effects. The first model results in approximately equal metal–metal distances along the chain (Scheme 1a), which hint to electronic delocalization.[16,17] On the other hand, the assumption of static disorder ("split-atom" model) affords an alternation of short ($d_<$) and long ($d_>$) distances (Scheme 1b and c), suggesting dimerization into pairs of quadruply-bonded chromium(II) ions.[18–21] This structural asymmetry, evaluated as $\Delta d = d_> - d_<$, ranges from 0.22 to 0.26 Å in solvatomorphs of **1**

[a]*Department of Chemical and Geological Sciences, University of Modena and Reggio Emilia & INSTM, I-41125 Modena, Italy. E-mail: acornia@unimore.it*
[b]*Department of Chemistry, University of Warwick, Gibbet Hill, Coventry, CV4 7AL, UK*
[c]*Department of Chemistry 'Ugo Schiff', University of Florence & INSTM, I-50019 Sesto Fiorentino (FI), Italy*

† Electronic supplementary information (ESI) available: Chemical scheme on the reactivity of mixtures of 2,6-dibromopyridine and 2,6-diaminopyridine (Scheme S1), further considerations on reaction mechanism (Supplementary Note 1 and Scheme S2), scale-expanded proton NMR spectra of H_2tpda, H_2tpda-d_2, and H_2tpda-d_4 (Fig. S1), proton NMR spectrum of H_2tpda-d_2 obtained by acidic H/D exchange (Fig. S2 and S3), full-range ESI-MS spectra of **2**, **2**-d_8 and **2**-d_{16} (Fig. S4). See DOI: 10.1039/c7dt03931j

‡ Current address: School of Physics, AMBER and CRANN, Trinity College, Dublin 2, Ireland.

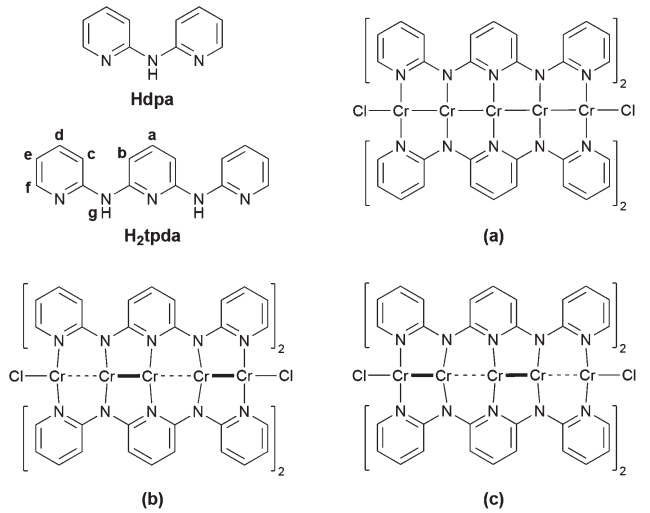

Scheme 1 Hdpa and H_2tpda ligands (with the hydrogen labelling scheme), and $[Cr_5(tpda)_4Cl_2]$ (**2**) complex in its symmetric (a) and unsymmetric (b, c) structures.

at −60 °C.[18] However, an illuminating structural study by Wu *et al.* has cast serious doubts on the validity of a "split-atom" model for the trichromium(II) string in **1**·Et_2O. At 15 K, this molecule adopts a symmetric structure in the solid state, with no evidence for static disorder.[22] These results are in complete agreement with Density Functional Theory (DFT) calculations, which indicate a symmetric gas-phase equilibrium structure for **1**[23] and its congeners, except for those containing very weak axial ligands (*e.g.* NO_3^-).[24] However, the central metal ion lies in a very shallow potential energy surface and distortion of the symmetric structure is an energetically facile process, thereby explaining the structural versatility of trichromium(II) strings.[18,25,26] In pentachromium(II) EMACs, as well as in their Cr_7 and Cr_9 congeners,[27,28] application of the "split-atom" model results in a much more pronounced structural asymmetry, with $d_< = 1.86$–2.03 Å, $d_> = 2.58$–2.66 Å and $\Delta d \sim 0.7$ Å in solvatomorphs of **2** at −60 °C.[19,20] These complexes seemingly feature formally quadruply-bonded Cr_2^{4+} units *plus* one terminal high-spin ($S = 2$) chromium(II) center, that in **2** exhibits a directionally-bistable magnetic moment and is at the origin of the observed SMM behaviour.[15]

Structural information on chromium-based EMACs without the rigid constraints of a crystal lattice is comparatively scarce,[29,30] although such studies are of importance to the field of single-molecule electronics. Within the series $[M_n(L)_4(SCN)_2]$ (M = Co, Ni for $n = 3, 5$; M = Cr for $n = 3, 5, 7$; L = oligo-α-pyridylamido ligand) the Cr derivatives are especially interesting in that they display the highest single-molecule conductance among strings of the same length.[4]

We have now performed DFT calculations and found that, at variance with its trichromium(II) congener **1**, complex **2** has an unsymmetric ground structure, although in the gas phase the symmetric form lies only 2.9 kcal mol^{-1} higher in energy. Such an energy difference becomes 3.9 kcal mol^{-1} when implicit solvent effects (CH_2Cl_2) are included. Next, we have used NMR methods and an isotopic labelling strategy to investigate the structure adopted by **2** in solution. To simplify the spectra and aid in peak assignment, we have first developed an improved Pd-free route to bulk quantities of H_2tpda (Scheme 1). Subsequently we have carried out post-synthetic isotopic labelling with deuterium on *b* positions only (H_2tpda-d_2) or on both *b* and *f* positions (H_2tpda-d_4). ^{1}H NMR spectroscopy has then been complemented with ^{2}H NMR on samples of **2**, $[Cr_5(tpda\text{-}d_2)_4Cl_2]$ (**2**-d_8) and $[Cr_5(tpda\text{-}d_4)_4Cl_2]$ (**2**-d_{16}) in dichloromethane solution. The results provide clear evidence that this pentachromium(II) complex has a symmetric (D_4) structure, meaning that it shuttles between the two unsymmetric forms at a rate faster than NMR timescale.

Experimental

General procedures

Chemicals were of reagent grade and were used as received, unless otherwise noted. D_2O (99.97 D%) and CD_3OD (99.8 D%) were used for H/D exchange experiments. All operations involving chromium(II) complexes were carried out inside an MBraun UniLAB glovebox using anhydrous solvents degassed by three freeze–pump–thaw cycles. Room temperature ^{1}H and ^{2}H NMR spectra were recorded at 400.13 and 61.42 MHz, respectively, on a Bruker Avance400 FT-NMR spectrometer. Proton chemical shifts are expressed in ppm downfield from Me_4Si as external standard, by setting the residual ^{1}H signal of DMSO-d_6 and CD_2Cl_2 at 2.50 and 5.32 ppm, respectively.[31] The chemical shift (ppm) axis in ^{2}H spectra was calibrated by setting the deuterium signal of DMSO and CH_2Cl_2 at 2.50 and 5.32 ppm, respectively. Spectra analysis was carried out with TopSpin 3.5 pl 7 software using the following processing parameters: SI = TD, LB = 0.05 (0.3) Hz for ^{1}H (^{2}H) spectra of the ligands, LB = 0.5 Hz for both ^{1}H and ^{2}H spectra of the complexes. *J* values are given in Hz. Isotopic enrichments were evaluated from proton spectra by setting the integrated area of H*e* signal equal to 2H. The intensity of this peak was always larger or equal to that of the remaining signals, indicating a negligible tendency of H*e* protons to undergo H/D exchange in the explored conditions. Spectra of **2**, **2**-d_8 and **2**-d_{16} complexes were recorded in valved 5 mm NMR tubes loaded inside the above mentioned glovebox (*ca.* 8–10 mg in 0.9–1.0 mL of solvent). In the case of **2**-d_8 and **2**-d_{16}, ^{2}H spectra in CH_2Cl_2 were first recorded, then the solvent was completely evaporated and the solid residue redissolved in CD_2Cl_2 for measuring ^{1}H spectra (signals from residual traces of chloroform and diethylether still appear in the spectra, but are neglected in the peak list). ESI-MS measurements were made in positive ion mode on an Agilent Technologies 6310A Ion Trap LC-MS(*n*) instrument by direct infusion of solutions in anhydrous and deoxygenated CH_2Cl_2. Isotopic patterns were simulated using Isotope Distribution Calculator.[32]

Synthesis and H/D exchange

H_2tpda. 2,6-Diaminopyridine (0.546 g, 5.00 mmol) and LiH (0.270 g, 34.0 mmol) were sequentially introduced in a 50 mL round bottomed flask under Ar and stirred for 5 min. A small condenser topped by a $CaCl_2$ tube was mounted and flushed with Ar, then 2-fluoropyridine (1.30 mL, 1.47 g, 15.1 mmol) and pyridine (2.6 mL) were added from the top using a pipette. After 5 min, the flask was immersed in an oil bath preheated at 150 °C and some minutes later (before the mixture became a solid mass) toluene (7.0 mL) was introduced. The mixture was stirred for 3 hours 15 min and then cooled down with a water bath. TLC (eluent CH_2Cl_2 : EtOH 9 : 1 + 3 drops of 30% aqueous ammonia) showed no 2,6-diaminopyridine (r.f. 0.34), traces of dimer **A** (see Scheme 2, r.f. 0.49) and a substantial amount of H_2tpda (r.f. 0.68). The solvent was removed under vacuum, water (40 mL) was added to the solid residue and the mixture was stirred for 10 min. Filtration through a Gooch funnel (porosity no. 3) followed by extensive washing (3 × 15 mL water + 2 × 20 mL hot water) afforded a wet beige solid. This was dissolved in THF (45 mL) and filtered on a short silica plug (1.0 g), which was washed with fresh THF (2 × 5 mL). Removal of all volatiles from the combined THF phases gave H_2tpda as a brownish solid (1.25 g, 95%) with excellent TLC purity. To gain further purification a practical digestion method was developed. In a 25 mL round bottom flask containing crude H_2tpda (1.25 g, 4.75 mmol), CH_3OH (5 mL), CH_2Cl_2 (5 mL) and Et_2O (5 mL) were added and the mixture left under stirring for 3 hours at room temperature. The flask was cooled in an ice bath, then the mixture was filtered through a Gooch funnel (porosity no. 3) and the collected solid washed with Et_2O (3 × 2 mL). After drying at a mechanical pump, purified H_2tpda was obtained (1.18 g, 94%, 90% overall) as a beige solid. Mp 222 °C. δH (400 MHz; DMSO-d_6; Me_4Si) 9.37 (2H, s, H*g*), 8.21 (2H, ddd, $^3J(f,e)$ = 4.9, $^4J(f,d)$ = 1.9, $^5J(f,c)$ = 0.8, H*f*), 7.83 (2H, ddd, $^3J(c,d)$ = 8.5, $^4J(c,e) \sim {}^5J(c,f) \sim$ 0.9, H*c*), 7.64 (2H, ddd, $^3J(d,c)$ = 8.5, $^3J(d,e)$ = 7.1, $^4J(d,f)$ = 1.9, H*d*), 7.50 (1H, t, $^3J(a,b)$ = 8.0, H*a*), 7.13 (2H, d, $^3J(b,a)$ = 8.0, H*b*), 6.85 (2H, ddd, $^3J(e,d)$ = 7.1, $^3J(e,f)$ = 4.9, $^4J(e,c)$ = 1.0, H*e*).

H_2tpda-d_2. H_2tpda (100 mg) and D_2O (1.55 mL) were introduced in a 2 mL stainless steel vessel and the screw cap closed. The vessel was placed in a preheated oven at 220 °C for 24 hours. After cooling, the yellowish-green solid material was recovered and washed with water (5 mL) to give a beige solid (83 mg, 82%). ^{1}H NMR analysis indicated 90.5% and 15.5% deuteration on *b* and *f* positions, respectively. Although H*c* and H*d* occur in two different environments, due to the small percentage of deuteration on *f* positions the minority component was difficult to resolve and was neglected in the assignments below. δH (400 MHz; DMSO-d_6; Me_4Si) 9.36 (2H, s, H*g*), 8.21 (1.69H, ddd, $^3J(f,e)$ = 4.9, $^4J(f,d)$ = 1.9, $^5J(f,c)$ = 0.8, H*f*), 7.83 (2H, ddd, $^3J(c,d)$ = 8.4, $^4J(c,e) \sim {}^5J(c,f) \sim$ 0.9, H*c*), 7.64 (2H, ddd, $^3J(d,c)$ = 8.4, $^3J(d,e)$ = 7.2, $^4J(d,f)$ = 1.9, H*d*), 7.50 (0.19H, d, $^3J(a,b)$ = 8.0, H*a* in molecules with one residual H*b*), 7.50 (0.81H, s, H*a* in molecules with no residual H*b*), 7.13 (0.19H, d, $^3J(b,a)$ = 8.0, H*b*), 6.85 (1.69H, ddd, $^3J(e,d)$ = 7.2, $^3J(e,f)$ = 4.9, $^4J(e,c)$ = 1.0, H*e* in pyridyl groups not deuterated on *f* position), 6.85 (0.31H, dd, $^3J(e,d)$ = 7.1, $^4J(e,c)$ = 1.0, H*e* in pyridyl groups deuterated on *f* position).

H_2tpda-d_2 (by acidic H/D exchange). D_2O (5.0 mL) was introduced in a test tube equipped with a ground joint and a septum. After cooling in an ice bath, distilled AcCl (1.0 mL, 1.1 g, 14 mmol) was added through the septum under stirring, the solution was allowed to warm up to room temperature and H_2tpda (50 mg, 0.19 mmol) was added to give a yellow solution. A condenser was mounted on top of the test tube and the solution was refluxed, with regular sampling (1.0 mL) every hour. The work up of each sampled fraction consisted in adding solid NaOH (*ca.* 0.3 g) until alkaline pH. The beige precipitate was filtered out, washed with water (1.0 mL) and Et_2O (1.0 mL) and dissolved in hot THF (1.5 mL). Removal of all volatiles *in vacuo* afforded a yellowish solid (total: 48 mg, 95%). ^{1}H NMR analysis indicated a high degree of deuteration of *b* positions (96.7%) already after 2 hours of reflux, with negligible H/D exchange on the remaining positions; after 4 hours a further increase of isotopic enrichment at *b* positions (98.1%) was accompanied by the onset of deuteration (few percent) at other hydrogen sites. δH (400 MHz; DMSO-d_6; Me_4Si) 9.36 (2H, s, H*g*), 8.21 (2H, ddd, $^3J(f,e)$ = 4.9, $^4J(f,d)$ = 1.9, $^5J(f,c)$ = 0.8, H*f*), 7.82 (2H, ddd, $^3J(c,d)$ = 8.5, $^4J(c,e) \sim {}^5J(c,f) \sim$ 0.9, H*c*), 7.63 (2H, ddd, $^3J(d,c)$ = 8.5, $^3J(d,e)$ = 7.1, $^4J(d,f)$ = 1.9, H*d*), 7.50 (0.065H, d, $^3J(a,b)$ = 8.0, H*a* in molecules with one residual H*b*), 7.50 (0.935H, s, H*a* in molecules with no residual H*b*), 7.12 (0.065H, d, $^3J(b,a)$ = 8.0, H*b*), 6.85 (2H, ddd, $^3J(e,d)$ = 7.1, $^3J(e,f)$ = 4.9, $^4J(e,c)$ = 1.0, H*e*).

H_2tpda-d_4. H_2tpda (56 mg), CD_3OD (0.10 mL) and D_2O (1.75 mL) were introduced in a 2 mL stainless steel vessel and the screw cap closed. The vessel was placed in a preheated

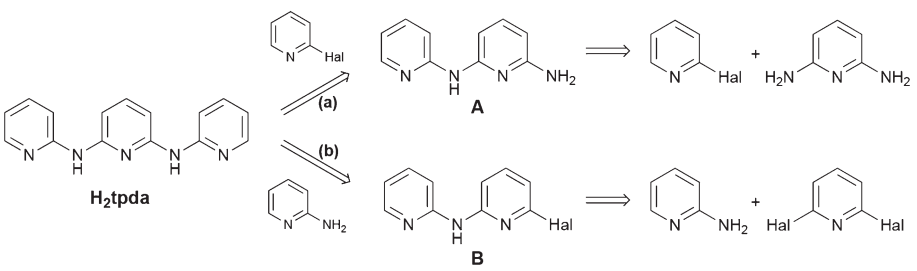

Scheme 2 Retrosynthetic approaches to H_2tpda.

oven at 230 °C for 24 hours. The same work-up described for H_2tpda-d_2 gave a beige solid (35 mg, 62%). ^{1}H NMR analysis indicated 98%, 83% and 4% deuteration on *b*, *f* and *c* positions, respectively. Three additional runs gave: 98% (*b*), 80% (*f*), 3% (*c*); 98% (*b*), 69% (*f*), 3% (*c*); 96% (*b*), 63% (*f*), 1% (*c*). 12.5, 26.0, 29.0 and 20.8 mg samples of deuterated H_2tpda from these four batches, respectively, were combined and used in subsequent reactions. The effect of partial deuteration of *c* positions on H*f* and H*e* resonances, as well as of residual H*f* protons on H*c*, H*d* and H*e* resonances could not be resolved and was neglected in the assignments below. δH (400 MHz; DMSO-d_6; Me_4Si) 9.36 (2H, s, H*g*), 8.21 (0.34H, ddd, $^3J(f,e)$ = 4.9, $^4J(f,d)$ = 1.9, $^5J(f,c)$ = 0.8, H*f*), 7.83 (1.91H, dd, $^3J(c,d)$ = 8.4, $^4J(c,e)$ = 0.9, H*c*), 7.64 (1.91H, dd, $^3J(d,c)$ = 8.4, $^3J(d,e)$ = 7.2, H*d* in pyridyl groups not deuterated on *c* position), 7.64 (0.09H, d, $^3J(d,e)$ = 7.2, H*d* in pyridyl groups deuterated on *c* position), 7.50 (0.034H, d, $^3J(a,b)$ = 8.0, H*a* in molecules with one residual H*b*), 7.50 (0.966H, s, H*a* in molecules with no residual H*b*), 7.13 (0.034H, d, $^3J(b,a)$ = 8.0, H*b*), 6.85 (2H, dd, $^3J(e,d)$ = 7.2, $^4J(e,c)$ = 0.9, H*e*). δD (61 MHz; DMSO; see above) 8.2 (2D, br s, D*f*), 7.1 (2D, br s, D*b*).

$[Cr_5(tpda)_4Cl_2]\cdot 4CHCl_3\cdot 2Et_2O$ (2·4CHCl$_3$·2Et$_2$O). The compound was prepared using the procedure described by Chang *et al.*[15,17] δH (400 MHz; CD_2Cl_2; Me_4Si) 13.0 (br), 7.32 (s, $CHCl_3$), 3.44 (q, CH_3CH_2O), 2.3 (br), 1.15 (t, CH_3CH_2O), 1.0 (br), 0.1 (br), −10.2 (br). ESI-MS: *m*/*z* 1376.2 ($[Cr_5(tpda)_4Cl_2]^+$, 100%), 1359.2 (4).

$[Cr_5(tpda\text{-}d_2)_4Cl_2]\cdot 4CHCl_3\cdot 2Et_2O$ (2-d_8·4CHCl$_3$·2Et$_2$O). H_2tpda-d_2 obtained by H/D exchange in D_2O (81 mg, 0.31 mmol), CD_3OD (1.3 mL) and THF (2.0 mL) were introduced in a conical flask. The mixture was heated to reflux until complete dissolution, then naphthalene (2.0 g) was added and the mixture heated to 100 °C for 1 hour to evaporate all volatiles. The flask was then cooled down to room temperature and $CrCl_2$ (58 mg, 0.47 mmol) and *t*BuOK (69 mg, 0.61 mmol) were added. The procedure for the reaction and the subsequent workup and crystallization were identical to those previously described for the nondeuterated analogue and the yield was comparable (~30%).[15,17] δH (400 MHz; CD_2Cl_2; Me_4Si) 13.0 (br), 2.3 (br), 0.1 (br), −10.2 (br). δD (61 MHz; CH_2Cl_2; see above) 0.85 (br). ESI-MS: *m*/*z* 1383.1 ($[Cr_5(tpda\text{-}d_2)_4Cl_2]^+$, 100%), 1366.1 (1).

$[Cr_5(tpda\text{-}d_4)_4Cl_2]\cdot 4CHCl_3\cdot 2Et_2O$ (2-d_{16}·4CHCl$_3$·2Et$_2$O). The synthesis also followed the above-described procedure, using: H_2tpda-d_4 (88 mg, 0.33 mmol) from four different batches, with average isotopic enrichment 97.5% (*b*), 72.8% (*f*), 2.7% (*c*); CD_3OD (1.5 mL), THF (2 mL), naphthalene (2.0 g), $CrCl_2$ (63 mg, 0.51 mmol) and *t*BuOK (76 mg, 0.68 mmol). The yield was comparable (~30%).[15,17] δH (400 MHz; CD_2Cl_2; Me_4Si) 13.0 (br), 2.4 (br), 0.1 (br), −10.2 (br). δD (61 MHz; CH_2Cl_2; see above) 0.82 (br). ESI-MS: *m*/*z* 1389.2 ($[Cr_5(tpda\text{-}d_4)_4Cl_2]^+$, 100%), 1371.2 (3).

Density functional theory (DFT) calculations

DFT calculations were performed with the ORCA program package, version 3.0.3.[33] Optimized geometries were computed using the PBE functional.[34] D3 dispersion corrections scheme[35] was also used. Scalar relativistically recontracted versions of the Ahlrichs triple-ζ basis set, def2-TZVP, were used on Cr, N, and Cl atoms while single-ζ basis set, def2-SVP, was used for C and H atoms.[36] The conductor-like screening model (COSMO)[37] was used to simulate a CH_2Cl_2 solution (ε = 9.08). The reason for performing the geometry optimizations within a model solvent was to exclude any solvent effect in the localization/delocalization of the Cr–Cr bonds. Resolution of identity (RI) was used to approximate two electron integrals. Considering that **2** spans a very flat potential energy surface, two different starting geometries were chosen: symmetric and unsymmetric arrangements of the Cr atoms. A tight convergence threshold was also used (TightOpt). The SCF calculations were tightly converged (TightSCF) with unrestricted spin (UKS). Numerical integrations during all DFT calculations were done on a dense grid (ORCA grid4) while the final run was also performed on a denser one (ORCA grid5).

Results and discussion

DFT calculations

Theoretical calculations in the gas phase were performed to shed light on the controversial structure of **2**.[17,19,20] Although CASSCF method would be preferable, the computational demand for a structure optimization at this level of theory would be too high and we thus recurred to DFT. The structure was optimized with both symmetric and unsymmetric distributions of metal centers as guess geometries, to be sure to start the optimization close to two possible different minima. For convenience, Cr atoms were numbered as Cr1, Cr2,...Cr5 along the chain, with Cr1 representing the formally "isolated" metal center in the unsymmetric structure. In spite of the shallow potential energy surface, DFT succeeded in finding two different stationary points. The unsymmetric structure (Fig. 1a) was found more stable than the symmetric one (Fig. 1b) by 2.9 kcal mol^{-1}. When solvent effects (CH_2Cl_2) were included through the COSMO model,[37] the difference in energy between the two stationary points increased by only 1 kcal mol^{-1} in favour of the unsymmetric form with no significant effect on structural parameters of interest, which are reported in Table 1. In the symmetric structure (Fig. 1b) the two inner Cr–Cr distances (Cr2–Cr3 and Cr3–Cr4) are shorter (2.20–2.22 Å) than Cr1–Cr2 and Cr4–Cr5 (2.31–2.32 Å). In the unsymmetric structure (Fig. 1a) the C_2 symmetry element located on Cr3 is lost and an alternation of short (1.85–1.90 Å) and long (2.55–2.61 Å) separations results, which matches the experimental interpretation of X-ray data using a "split-atom" model.[19,20] It is worth mentioning that the computed value of about 1.9 Å for the shortest Cr–Cr separation is in agreement with the usual distance associated to a formally fourth-order Cr–Cr bond.[38]

The computed spin densities (Lödwin analysis) and S^2 expectation values are presented in Table 2. The alternating signs and the magnitudes of the spin densities, which depend

Table 1 Cr–Cr distances (Å) in solvatomorphs of **2**, as experimentally found in the solid state at 213 K and as resulting from DFT calculations

	Cr1–Cr2	Cr2–Cr3	Cr3–Cr4	Cr4–Cr5	Ref.
2·CH_2Cl_2	2.578(7)	1.901(6)	2.587(6)	2.031(6)	19
2·Et_2O	2.661(3)	1.862(3)	2.644(3)	1.931(3)	20
2·4$CHCl_3$·2Et_2O	2.598(3)	1.872(2)	2.609(2)	1.963(3)	20
DFT – symmetric (gas phase)	2.319	2.207	2.221	2.308	This work
DFT – unsymmetric (gas phase)	2.550	1.862	2.606	1.904	This work
DFT – symmetric (CH_2Cl_2)	2.308	2.205	2.220	2.318	This work
DFT – unsymmetric (CH_2Cl_2)	2.550	1.852	2.612	1.880	This work

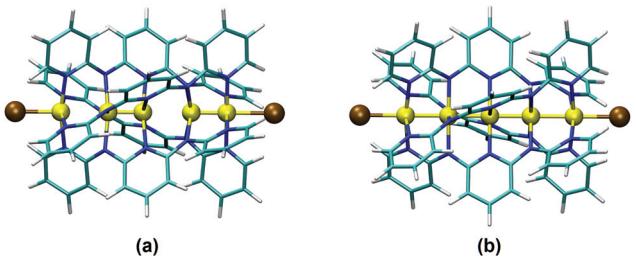

Fig. 1 Optimized structures of **2**: unsymmetric (a) and symmetric (b). Colour code: yellow = Cr, brown = Cl, blue = N, cyan = C, white = H. Metal centers are numbered as Cr1, Cr2,...Cr5 from left to right.

Table 2 Spin densities (Lödwin analysis) and S^2 expectation values in **2** as resulting from DFT calculations

	Cr1	Cr2	Cr3	Cr4	Cr5	$\langle S^2 \rangle$
DFT – symmetric (gas phase)	3.10	−2.45	2.50	−2.44	3.12	10.46
DFT – unsymmetric (gas phase)	3.40	−1.40	1.60	−1.54	1.73	8.04
DFT – symmetric (CH_2Cl_2)	3.13	−2.47	2.51	−2.46	3.14	10.49
DFT – unsymmetric (CH_2Cl_2)	3.44	−1.37	1.56	−1.45	1.62	7.94

on the symmetry of the molecule, support the orbital symmetry breaking. They clearly picture the consequences of an unsymmetric *vs.* symmetric configuration on the electronic structure. In the symmetric case, the spin densities are almost homogeneous in absolute value among the five metal centers, but slightly higher on the terminal ions. On the contrary, in the unsymmetric structure about 3.5 unpaired electrons are localized on Cr1 while only about 1.5 unpaired electrons are present on each of the remaining metal centers. The amount of spin density left on Cr2, Cr3, Cr4 and Cr5 suggests that a bond order larger than three is unlikely to occur within the formally quadruply-bonded Cr2,Cr3 and Cr4,Cr5 pairs. However, a significantly higher bond localization is apparent with respect to the symmetric case. Such a scenario is confirmed by the computed $\langle S^2 \rangle$ values, which are *ca.* 10.5 for the symmetric structure and *ca.* 8.0 for the unsymmetric one. These values have to be compared with those expected using computed spin densities[39a] (or, in alternative, formal spins),[39b] which are 10.46 (10.75) and 8.42 (8.75) for the symmetric and unsymmetric structures, respectively. The lower computed values for the unsymmetric structures can be explained by the increased deviation from a complete localization of the spins (*i.e.* increased overlap).[39a]

An improved metal-free synthesis of H_2tpda. Although the first H_2tpda-based EMACs were isolated by Peng's group as early as in 1997,[40] an efficient and reliable method to prepare H_2tpda is still publicly unavailable. In principle, two different synthetic schemes based on nucleophilic aromatic substitution (S_NAr) reactions can be identified (Scheme 2), which differ in one important respect.

In path (**b**), the intermediate **B** will hardly proceed to H_2tpda through an S_NAr mechanism, as its electrophilicity is lowered by the electrodonating arylamino substituent. By contrast, in path (**a**) the same electronic effect is expected to enhance the nucleophilicity of the primary amino group of intermediate **A**, that should promptly react to yield the target compound (these considerations do not apply to Pd-catalyzed reactions, which were in fact predominantly carried out following path (**b**), *vide infra*). Literature data on the reactivity of 2,6-dibromopyridine with 2,6-diaminopyridine (Scheme S1†) confirm this view.[41,42] The available procedures for the synthesis of H_2tpda indeed follow path (**a**) by reacting 2,6-diaminopyridine with overstoichiometric 2-halopyridine (Hal = Cl, Br) and an added base (*t*BuOK or NaH) in refluxing benzene or THF.[40,43–46] Although 2-chloropyridine gives better results, yields never exceed 60% even using a large excess of arylant. The acute inhalation and dermal toxicity of 2-chloropyridine makes this route even less appealing.

It is known that key factors for an efficient *N*-arylation of 2-aminopyridines with 2-halo or 2-alkoxypyridines are an appropriate choice of the base and of the solvent.[47,48] Sometimes microwave irradiation is helpful,[49,50] but the most popular way to improve the process is to use a Pd-catalyzed cross coupling method (Buchwald–Hartwig amination).[51,52] In fact, this reaction was extensively applied to the synthesis of oligo-α-pyridylamines and related ligands,[10,12,28,53–58] including H_2tpda itself (though details were not provided).[59]

Looking for a Pd-free approach to the synthesis of H_2tpda, we decided to explore the reactivity of 2-fluoropyridine, which is less toxic than 2-chloropyridine and is a known efficient electrophile in S_NAr reactions with anilines or other amines.[60–63] The order of addition of the reagents was inspired by the best available method, namely the synthesis of Br_2H_2tpda.[42] Thus,

the selected base (10 equiv.) was added to solid 2,6-diaminopyridine under Ar and stirred for 10 min at room temperature. Then 2-fluoro or 2-chloropyridine (4.0 equiv.) and the solvent (10 mL $mmol^{-1}$ of 2,6-diaminopyridine) were sequentially added and the reaction mixture was heated at reflux for 6 h, with final monitoring by TLC. From our survey, we concluded that 2-fluoropyridine converts 2,6-diaminopyridine more efficiently than 2-chloropyridine, while *t*BuOK and alkali–metal hydrides (LiH, NaH) are superior to other bases like Na_2CO_3, K_3PO_4,[47,48] NaOH, NaOEt or Na^0. Contrary to our reference literature report,[42] THF did not perform well with respect to toluene, DMSO or DMF (probably due to its lower boiling point) and toluene was finally selected to simplify reaction workup.

We further discovered that the addition of pyridine (py) as co-solvent in the reaction between 2,6-diaminopyridine, 2-fluoropyridine and LiH in toluene causes vigorous hydrogen evolution upon heating. Further experimentation indicated that py is an essential ingredient, as it promotes the formation of intermediate **A** (Scheme 2) even at room temperature, and permits its conversion to H_2tpda upon heating.§ Final refinements brought the method at its best (3.0 equiv. of 2-fluoropyridine, 3 hours 15 min of reaction time, minimal tar formation), although the role played by py is still unclear (see ESI Note 1†). The crude material is a brownish solid which can be purified by digestion, affording spectroscopically pure H_2tpda as a beige solid with excellent overall yield (90%). The room temperature ^{1}H NMR spectrum in DMSO-d_6, presented in Fig. 2a, shows seven signals and is thus consistent with C_{2v} molecular symmetry in solution; chemical shifts and multiplicities compare well with available literature data[46] (spectral data in ref. 44 are in part erroneous).

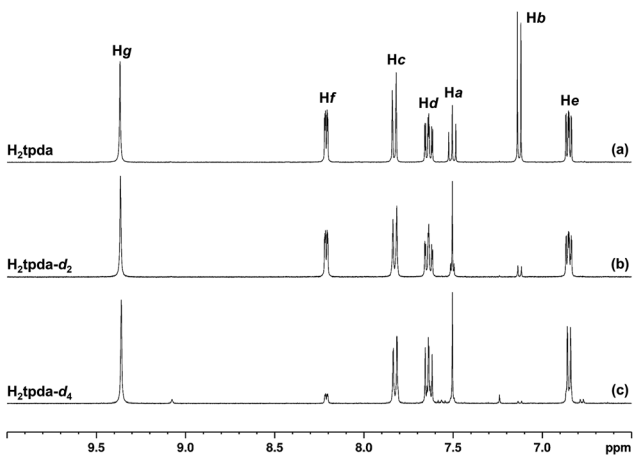

Fig. 2 Proton NMR spectra of H_2tpda (a), H_2tpda-d_2 (b) and H_2tpda-d_4 (c) in DMSO-d_6. For the labelling scheme, see Scheme 1.

§ Neither replacing py with more basic 2-ethylpyridine or 2,6-lutidine, nor adding small amounts of 4-(dimethylamino)pyridine improved the results.

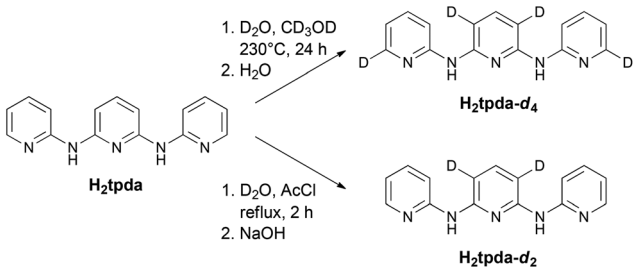

Scheme 3 Post-synthetic isotopic labelling of H_2tpda.

Post-synthetic isotopic labelling of H_2tpda

Although deutero-debromination of Br_2H_2tpda[64] might provide a route to the selective deuteration of H_2tpda on *f* positions, we preferred to test post-synthetic labelling (Scheme 3). H/D exchange was first monitored following prolonged heating at 220–230 °C in a 400-fold excess of D_2O inside a pressure resistant stainless steel vessel with a screw cap.[65] The product was obtained as a beige solid in good yield by washing the raw reaction mixture with water to remove some decomposition product visible in TLC (this treatment causes partial back exchange of N–D groups to N–H; deuteration of amino groups can be restored by boiling in CD_3OD and evaporating the solvent). These trials showed that both H*b* and H*f* hydrogens (Scheme 1) undergo exchange, as evident from the reduced intensity of the corresponding ^{1}H NMR peaks at 7.13 and 8.21 ppm in DMSO-d_6.

We also found that *b* positions exchange faster than *f* positions. Considering that acidic H/D exchange should follow an S_EAr mechanism, the high conjugation between the central pyridine ring and two arylamino substituents is likely to play a role.[66] However, using pure D_2O as a reaction medium gave poorly reproducibility, presumably due to the low solubility of H_2tpda in water. Addition of 5–6% (v/v) of CD_3OD as co-solvent was beneficial and afforded 96–98 D% at *b* and 63–83 D% at *f* positions (Scheme 3). The spectrum of a typical H_2tpda-d_4 sample in DMSO-d_6 is shown in Fig. 2c, while scale-expanded spectra are available in Fig. S1.† Beyond directly affecting the intensity of H*b* and H*f* signals, deuteration results in a clear modification of the hyperfine coupling patterns for neighboring protons. The hyperfine pattern for H*c* protons at 7.83 ppm, for instance, changes from a doublet-of-pseudo-triplets ($^3J(c,d) \gg {}^4J(c,e) \sim {}^5J(c,f)$) to a doublet-of-doublets upon deuteration of *f* positions. Similarly, the ddd pattern of H*e* protons at 6.85 ppm ($^3J(e,d) > {}^3J(e,f) > {}^4J(e,c)$) turns into a simpler dd. Finally, the triplet of H*a* protons in nondeuterated H_2tpda (7.50 ppm) becomes a singlet upon deuteration of *b* positions. The H*c* integrated intensity ranged from 1.99 to 1.91H, signalling that isotopic enrichment up to a few percent can also occur at these positions.

Deuteron NMR spectroscopy provided complementary information on H/D exchange. The H_2tpda-d_4 sample that afforded the spectrum in Fig. 2c, dissolved in nondeuterated DMSO, gave two main ^{2}H resonances at 8.2 and 7.1 ppm, with

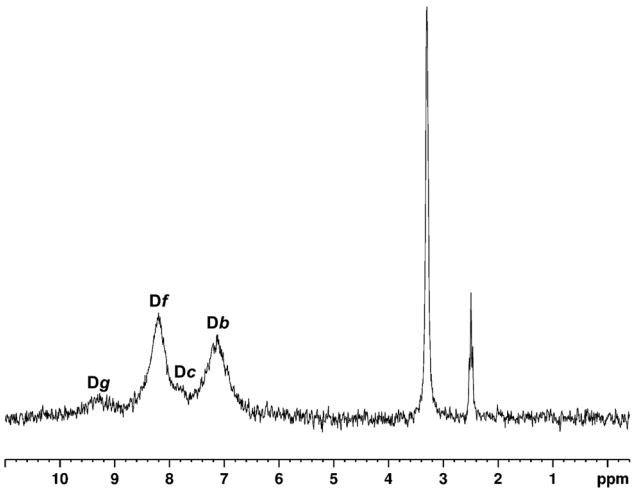

Fig. 3 Deuteron NMR spectra of H_2tpda-d_4 in DMSO. The sharp peaks at 2.50 and 3.30 ppm arise from deuterium naturally present in DMSO and water.

FWHM of 20–25 Hz (Fig. 3). By direct comparison with the chemical shift values in proton spectra, the two peaks are assigned to D*f* and D*b* nuclei, respectively, while the shoulder at 7.8 ppm confirms that H*c* hydrogens also undergo minor H/D exchange. Finally, the weak broad peak at 9.3 ppm is attributed to residual N–D groups.

Occasionally, using a 200-fold molar excess of D_2O we reached 90.5 and 15.5 D% on *b* and *f* positions, respectively (H_2tpda-d_2, see Fig. 2b and Fig. S1†). A similar selective exchange of *b* positions was later shown to occur by simply refluxing H_2tpda with a solution of DCl in AcOD/D_2O 1 : 5 (v/v) for 2 hours (Scheme 3 and Fig. S2 and S3†).

Solution properties of $[Cr_5(tpda)_4Cl_2]$ (2), $[Cr_5(tpda\text{-}d_2)_4Cl_2]$ (2-d_8) and $[Cr_5(tpda\text{-}d_4)_4Cl_2]$ (2-d_{16})

Crystalline samples of pentachromium(II) strings **2**, **2**-d_8 and **2**-d_{16} were prepared as tetrakis(chloroform) bis(diethylether) solvates following literature procedures.[15,17] Synthetic conditions require refluxing the reaction mixture in boiling naphthalene for several hours and might lower the isotopic enrichment of the ligand. Therefore, the crystalline material so obtained was preliminarily characterized by ESI-MS in CH_2Cl_2. Scale expanded spectra are compared in Fig. 4 (full scale spectra are available in Fig. S4†). The molecular ion peaks are detected at *m*/*z* = 1376.2, 1383.1 and 1389.2, respectively, confirming increasing isotopic enrichment across the series. The isotopic patterns were analyzed by assuming that only *b* positions are susceptible of H/D back exchange. The H/D ratios at the remaining positions were thus held fixed at the values determined by proton NMR (see Experimental section). The best agreement with experimental patterns is achieved with 70 and 96 D% at *b* positions in **2**-d_8 and **2**-d_{16}, respectively, indicating good to excellent persistence of D content.

Solutions of **2** in dichloromethane are indefinitely stable at room temperature in the absence of dioxygen. The ^{1}H NMR spectrum of a solution of **2** in CD_2Cl_2 is shown in Fig. 5a.

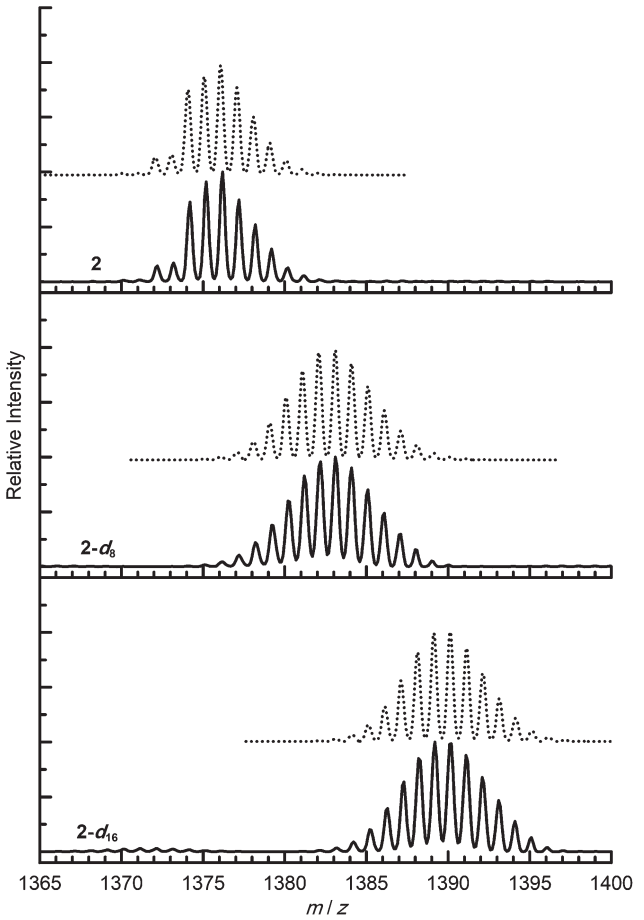

Fig. 4 Scale expanded ESI-MS spectra of **2**, **2**-d_8 and **2**-d_{16} (direct infusion, CH_2Cl_2, positive ion mode). Each graph shows the comparison between the experimental (solid line) and simulated (dotted line) isotopic patterns of molecular ion peaks at *m*/*z* = 1376.2, 1383.1 and 1389.2 (from top to bottom).

Beside narrow peaks arising from solvent residuals and other impurities, the spectrum is dominated by five very broad (10^2–10^3 Hz) and paramagnetically-shifted resonances of ligand protons at 13.0, 2.3, 1.0, 0.1 and −10.2 ppm. No other peaks are visible in a spectral window ranging from −80 to 80 ppm.

As shown in Scheme 1 and Fig. 2a, H_2tpda ligand in solution contains six magnetically inequivalent C–H protons[67] (*vs.* four in Hdpa). Assuming that the complex has at least fourfold symmetry in solution, *i.e.* that the four $tpda^{2-}$ ligands are equivalent, the expected number of resonances is *six* for a symmetric (over NMR timescale) D_4 structure and *eleven* for an unsymmetric C_4 one. This is exactly the number of NMR resonances detected for $[Ni_5(tpda)_4(SCN)_2]$ and $[NiRu_2Ni_2(tpda)_4(SCN)_2]$, which have symmetric and unsymmetric frameworks, respectively.[67] An unsymmetric structure would also entail a highly nonuniform spin density along the chain, with a localized high-spin (S = 2) chromium(II) center at one extreme and two formally quadruply-bonded Cr_2^{4+} pairs towards the other extreme. The dichromium(II) paddlewheel complex $[Cr_2(dpa)_4]$ contains one such pair and is a virtually

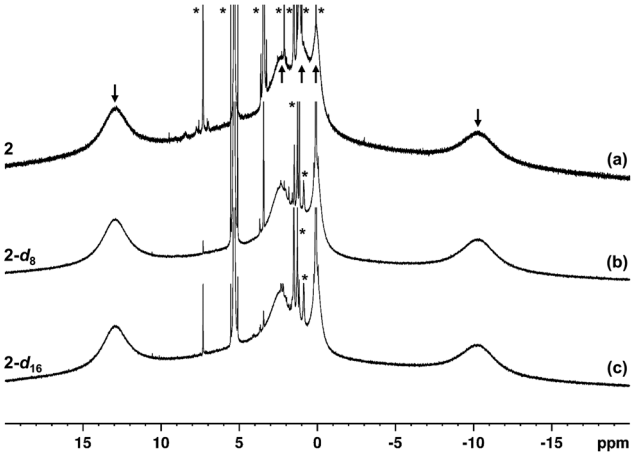

Fig. 5 ^{1}H NMR spectra of **2** (a), **2**-d_8 (b) and **2**-d_{16} (c) in CD_2Cl_2. Arrows in (a) mark the five broad peaks arising from tpda^{2-} protons. The narrow peaks labelled by asterisks in (a) arise from (in order of decreasing chemical shift): $CHCl_3$, $CHDCl_2$, Et_2O (CH_2), acetone, Et_2O (CH_3), water and silicone grease. The additional asterisked peaks in (b) and (c) are attributed to traces of *n*-hexane.

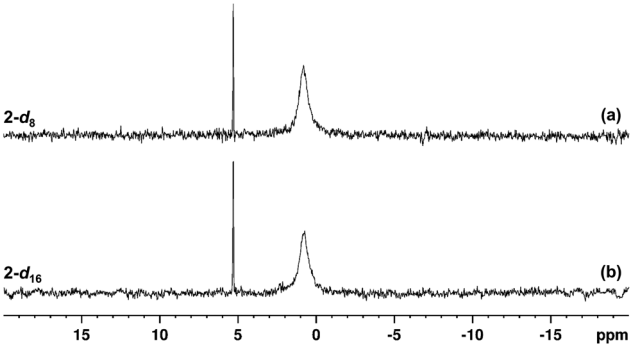

Fig. 6 Deuteron NMR spectra of **2**-d_8 (a) and **2**-d_{16} (b) in CH_2Cl_2. The sharp peak at 5.32 ppm arises from deuterium naturally present in CH_2Cl_2.

diamagnetic molecule. By consequence, its proton NMR signals are detected in the usual range for aromatic C–H groups and give resolvable hyperfine splittings.[68] The number, width, and chemical shift of the observed proton NMR resonances coherently suggest that **2** is symmetric over NMR timescale and that one resonance out of six is paramagnetically broadened beyond detection. This missing resonance is presumably that from *ortho*-pyridyl protons H*f*, which lie closest to the paramagnetic centers. This interpretation is confirmed by the ^{1}H NMR spectra of **2**-d_8 and **2**-d_{16} in CD_2Cl_2 (Fig. 5b and c). The two spectra feature the same ligand peaks as in Fig. 5a, except for the signal around 1.0 ppm, which is strongly reduced in intensity. The observation that deuteration of *f* positions has no impact on proton spectra proves that *ortho*-pyridyl protons are undetectable. ^{2}H NMR spectroscopy on the same samples of Fig. 5b and c in CH_2Cl_2 lends even more direct support to the proposed scenario. For both isotopic enrichments, a single paramagnetically-shifted resonance is detected at 0.8–0.9 ppm (Fig. 6), hence close to the position of the ^{1}H peak that disappears upon deuteration of *b* positions. Notice that such a resonance has a FWHM of *ca.* 40 Hz and is thus significantly sharper than found in proton spectra, a known advantage of ^{2}H over ^{1}H NMR spectroscopy for the investigation of paramagnetic systems.[69] The observation of a single peak of D*b* nuclei is also consistent with a symmetric (D_4) structure over NMR timescale. In fact, for an unsymmetric (C_4) structure featuring an alternation of long and short Cr–Cr separations (as in the solid state) the two D*b* nuclei of each ligand would be inequivalent and would give two distinct signals. One possibility is that the structure is truly symmetric in solution (Scheme 1a). This option is however ruled out by our DFT studies, which indicate that the ground state of **2** entails an alternation of long and short Cr–Cr distances. We contend that fast oscillation between the two equivalent unsymmetric structures (Scheme 1b and c) affords average D_4 symmetry and explains all our experimental results. Taking the energy difference between symmetric and unsymmetric forms (3.9 kcal mol^{-1} in CH_2Cl_2) as the activation energy for the interconversion, the oscillation rate at room temperature is expected to be much faster than the chemical shift difference between the observed NMR signals (*ca.* 10–20 ppm, *i.e.* 4000–8000 Hz at 400 MHz). The fast exchange regime is thus attained and the oscillation is averaged out over NMR timescale.[70]

Conclusions

With our study, we have demonstrated the applicability of isotopic (D) labelling and solution ^{1}H/^{2}H NMR spectroscopies to probe the structure of paramagnetic EMACs of relevance in molecular electronics and magnetism, such as $[Cr_5(tpda)_4Cl_2]$ (**2**). A reliable, Pd-free synthetic route has been developed to prepare H_2tpda from 2,6-diaminopyridine and 2-fluoropyridine, with yield (90%) largely surpassing that of the best published methods.[43–46] H/D exchange procedures have then been devised to allow deuteration at *b* positions only (H_2tpda-d_2), or at both *b* and *f* positions (H_2tpda-d_4, see Scheme 1). The complementary information provided by ^{1}H and ^{2}H NMR spectra of **2**, **2**-d_8 and **2**-d_{16} in dichloromethane demonstrates that *ortho*-pyridyl hydrogens are undetectable in these complexes, presumably due to their close proximity to the paramagnetic centers. The five paramagnetically-broadened and shifted signals observed in proton spectra, *plus* this invisible resonance, exactly match the number of inequivalent hydrogens expected for a symmetric (D_4) structure.

Similar spectroscopic features have been reported for trichromium(II) complex $[Cr_3(dpa)_4(N_3)_2]$ (**3**).[26] From room-temperature to −50 °C only *three* resonances of dpa$^-$ protons are observed in the ^{1}H NMR spectrum of **3**·Et_2O in CD_2Cl_2 solution.[26] In these complexes of dpa$^-$, a symmetric (D_4) structure would afford *four* inequivalent protons, while an unsymmetric (C_4) structure would contain *eight* inequivalent protons. The authors argued that a symmetric structure is most probably adopted over the timescale of NMR experiment, with one

signal paramagnetically shifted and broadened beyond detection (based on our results, the signal from *ortho*-pyridyl protons). DFT calculations have shown that in trichromium(II) EMACs (except those containing very weak axial ligands) the asymmetric stretching of the Cr_3 unit is a very soft mode and that the potential energy surface features a single minimum corresponding to the *symmetric* structure.[23,24] The symmetry emerging from NMR spectra thus reflects the actual ground symmetry of **3**, although a large asymmetric stretching amplitude is expected.

At difference with this, DFT studies on **2** in the gas phase and including CH_2Cl_2 solvent effects indicate that the two equivalent unsymmetric forms are more stable (by 2.9 and 3.9 kcal mol^{-1}, respectively) than the symmetric one; by consequence, the high symmetry displayed by **2** in dichloromethane is explained by a hopping processes occurring at a rate faster than NMR timescale. In spite of their different energy landscapes, then, strings **2** and **3** both display their maximum possible symmetry (D_4) on the timescale of NMR experiment.

It remains to be elicited if the symmetric and unsymmetric forms of **2** may be stable as separate, slowly switching entities, as postulated to explain the bimodal single-molecule conductance of $[Cr_5(tpda)_4(SCN)_2]$.[4] In STM break-junction experiments,[4b] two sets of conductance values were found, namely $48.8(1.0) \times 10^{-4}$ and $9.5(1.2) \times 10^{-4}$ G_0 (G_0 is the conductance quantum), which were assigned to the symmetric (delocalized, more conducting) and unsymmetric (localized, less conducting) forms, respectively. The heptachromium(II) congener also exhibits two conductance values.[4a] However, low-symmetry distortions do not necessarily have such a large impact on electron transport, and DFT calculations on trichromium(II) EMACs have indeed predicted an opposite trend.[2,3c] More important, precise structural information on the existence of pentachromium(II) strings in symmetric form is still lacking. Based on surface-enhanced Raman spectra, the two isomers were claimed to coexist when molecules are bound to metal nanoparticles in solution, but without solid experimental evidence.[29] In fact, contrary to the assertion made in ref. 29, the X-ray data in ref. 17 (Peng's group) and ref. 21 (Cotton's group) do not show the existence of both symmetric and unsymmetric forms; rather, these and other papers[19,20] discuss two distinct structural models which differ for the *neglection*[17] or *inclusion*[19–21] of positional disorder effects. That positional disorder may be present is suggested by the otherwise distinctly prolate displacement ellipsoids of the Cr ions along the chain axis and by the lower wR_2 index achieved using a "split atom" model.[21] We cannot at present exclude that, under special circumstances not captured by our DFT calculations, a symmetric complex may become stable in the solid state. However, since our DFT studies indicate that in the gas phase and in solution the symmetric form has a distinctly higher energy than the unsymmetric one, the existence of a stable symmetric complex without the rigid constraints of a crystal lattice would be, in our view, quite surprising.

Conflicts of interest

There are no conflicts to declare.

Acknowledgements

A. D. gratefully acknowledges the University of Warwick (UK) for an Erasmus+ Placement fellowship during his work in Modena (Italy). A. L. and F. T. thank the European Research Council for funding through the Advanced Grant MolNanoMaS (no. 267746). A. C. is grateful to A. Mucci (Department of Chemical and Geological Sciences) for stimulating discussion on dynamic NMR spectroscopy.

Notes and references

1 Y. Tanaka, M. Kiguchi and M. Akita, *Chem. – Eur. J.*, 2017, **23**, 4741–4749.
2 V. P. Georgiev, P. J. Mohan, D. DeBrincat and J. E. McGrady, *Coord. Chem. Rev.*, 2013, **257**, 290–298.
3 (*a*) P. J. Mohan, V. P. Georgiev and J. E. McGrady, *Chem. Sci.*, 2012, **3**, 1319–1329; (*b*) V. P. Georgiev, W. M. C. Sameera and J. E. McGrady, *J. Phys. Chem. C*, 2012, **116**, 20163–20172; (*c*) V. P. Georgiev and J. E. McGrady, *J. Am. Chem. Soc.*, 2011, **133**, 12590–12599.
4 (*a*) I.-W. P. Chen, M.-D. Fu, W.-H. Tseng, J.-Y. Yu, S.-H. Wu, C.-J. Ku, C.-h. Chen and S.-M. Peng, *Angew. Chem., Int. Ed.*, 2006, **45**, 5814–5818; (*b*) T.-C. Ting, L.-Y. Hsu, M.-J. Huang, E.-C. Horng, H.-C. Lu, C.-H. Hsu, C.-H. Jiang, B.-Y. Jin, S.-M. Peng and C.-h. Chen, *Angew. Chem., Int. Ed.*, 2015, **54**, 15734–15738.
5 (*a*) K. Uemura, *Dalton Trans.*, 2017, **46**, 5474–5492; (*b*) G. Aromí, *Comments Inorg. Chem.*, 2011, **32**, 163–194.
6 J. F. Berry, F. A. Cotton, L. M. Daniels, C. A. Murillo and X. Wang, *Inorg. Chem.*, 2003, **42**, 2418–2427.
7 J. F. Berry, *Struct. Bonding*, 2010, **136**, 1–28.
8 (*a*) S.-A. Hua, M.-C. Cheng, C.-h. Chen and S.-M. Peng, *Eur. J. Inorg. Chem.*, 2015, 2510–2523; (*b*) S.-A. Hua, Y.-C. Tsai and S.-M. Peng, *J. Chin. Chem. Soc.*, 2014, **61**, 9–26.
9 I. P.-C. Liu, W.-Z. Wang and S.-M. Peng, *Chem. Commun.*, 2009, 4323–4331.
10 H. Hasanov, U.-K. Tan, R.-R. Wang, G. H. Lee and S.-M. Peng, *Tetrahedron Lett.*, 2004, **45**, 7765–7769.
11 R. H. Ismayilov, W.-Z. Wang, G.-H. Lee, C.-Y. Yeh, S.-A. Hua, Y. Song, M.-M. Rohmer, M. Bénard and S.-M. Peng, *Angew. Chem., Int. Ed.*, 2011, **50**, 2045–2048.
12 P.-J. Chen, M. Sigrist, E.-C. Horng, G.-M. Lin, G.-H. Lee, C.-h. Chen and S.-M. Peng, *Chem. Commun.*, 2017, **53**, 4673–4676.
13 D. W. Brogden and J. F. Berry, *Comments Inorg. Chem.*, 2016, **36**, 17–37.

14 J. H. Christian, D. W. Brogden, J. K. Bindra, J. S. Kinyon, J. van Tol, J. Wang, J. F. Berry and N. S. Dalal, *Inorg. Chem.*, 2016, **55**, 6376–6383.
15 A. Cornia, L. Rigamonti, S. Boccedi, R. Clérac, M. Rouzières and L. Sorace, *Chem. Commun.*, 2014, **50**, 15191–15194.
16 R. Clérac, F. A. Cotton, L. M. Daniels, K. R. Dunbar, C. A. Murillo and I. Pascual, *Inorg. Chem.*, 2000, **39**, 748–751.
17 H.-C. Chang, J.-T. Li, C.-C. Wang, T.-W. Lin, H.-C. Lee, G.-H. Lee and S.-M. Peng, *Eur. J. Inorg. Chem.*, 1999, 1243–1251.
18 J. F. Berry, F. A. Cotton, T. Lu, C. A. Murillo, B. K. Roberts and X. Wang, *J. Am. Chem. Soc.*, 2004, **126**, 7082–7096.
19 F. A. Cotton, L. M. Daniels, T. Lu, A. Murillo and X. Wang, *J. Chem. Soc., Dalton Trans.*, 1999, 517–518.
20 F. A. Cotton, L. M. Daniels, C. A. Murillo and X. Wang, *Chem. Commun.*, 1999, 2461–2462.
21 J. F. Berry, F. A. Cotton, C. S. Fewox, T. Lu, C. A. Murillo and X. Wang, *Dalton Trans.*, 2004, 2297–2302.
22 L.-C. Wu, M. K. Thomsen, S. R. Madsen, M. Schmoekel, M. R. V. Jørgensen, M.-C. Cheng, S.-M. Peng, Y.-S. Chen, J. Overgaard and B. B. Iversen, *Inorg. Chem.*, 2014, **53**, 12489–12498.
23 N. Benbellat, M.-M. Rohmer and M. Bénard, *Chem. Commun.*, 2001, 2368–2369.
24 M. Spivak, V. Arcisauskaite, X. López, J. E. McGrady and C. de Graaf, *Dalton Trans.*, 2017, **46**, 6202–6211.
25 R. H. Ismayilov, W.-Z. Wang, G.-H. Lee, R.-R. Wang, I. P.-C. Liu, C.-Y. Yeh and S.-M. Peng, *Dalton Trans.*, 2007, 2898–2907.
26 Y. Turov and J. F. Berry, *Dalton Trans.*, 2012, **41**, 8153–8161.
27 R. H. Ismayilov, W.-Z. Wang, G.-H. Lee, C.-H. Chien, C.-H. Jiang, C.-L. Chiu, C.-Y. Yeh and S.-M. Peng, *Eur. J. Inorg. Chem.*, 2009, 2110–2120.
28 R. H. Ismayilov, W.-Z. Wang, R.-R. Wang, C.-Y. Yeh, G.-H. Lee and S.-M. Peng, *Chem. Commun.*, 2007, 1121–1123.
29 Y.-M. Huang, H.-R. Tsai, S.-H. Lai, S. J. Lee, I.-C. Chen, C. L. Huang, S.-M. Peng and W.-Z. Wang, *J. Phys. Chem. C*, 2011, **115**, 13919–13926.
30 C.-J. Hsiao, S.-H. Lai, I.-C. Chen, W.-Z. Wang and S.-M. Peng, *J. Phys. Chem. A*, 2008, **112**, 13528–13534.
31 G. R. Fulmer, A. J. M. Miller, N. H. Sherden, H. E. Gottlieb, A. Nudelman, B. M. Stoltz, J. E. Bercaw and K. I. Goldberg, *Organometallics*, 2010, **29**, 2176–2179.
32 J. E. Redman, *Isotope Distribution Calculator*, Cardiff University, Cardiff, UK, 2005, http://www.kombyonyx.com/isotopes/ (accessed October 2017).
33 F. Neese, The ORCA program system, *Wiley Interdiscip. Rev.: Comput. Mol. Sci.*, 2012, **2**, 73–78.
34 J. P. Perdew, K. Burke and M. Ernzerhof, *Phys. Rev. Lett.*, 1996, **77**, 3865–3868.
35 S. Grimme, J. Antony, S. Ehrlich and H. Krieg, *J. Chem. Phys.*, 2010, **132**, 154104.
36 (*a*) D. A. Pantazis, X.-Y. Chen, C. R. Landis and F. Neese, *J. Chem. Theory Comput.*, 2008, **4**, 908–919; (*b*) F. Weigend and R. Ahlrichs, *Phys. Chem. Chem. Phys.*, 2005, **7**, 3297–3305.
37 A. Klamt and G. Schüürmann, *J. Chem. Soc., Perkin Trans. 2*, 1993, 799–805.
38 M. Brynda, L. Gagliardi and B. O. Roos, *Chem. Phys. Lett.*, 2009, **471**, 1–10.
39 (*a*) A. Bencini and F. Totti, *J. Chem. Theory Comput.*, 2009, **5**, 144–154; (*b*) A. Bencini and F. Totti, *Int. J. Quantum Chem.*, 2005, **101**, 819–825.
40 S.-J. Shieh, C.-C. Chou, G.-H. Lee, C.-C. Wang and S.-M. Peng, *Angew. Chem., Int. Ed. Engl.*, 1997, **36**, 56–59.
41 H. Hasan, U.-K. Tan, Y.-S. Lin, C.-C. Lee, G.-H. Lee, T.-W. Lin and S.-M. Peng, *Inorg. Chim. Acta*, 2003, **351**, 369–378.
42 H.-Y. Gong, X.-H. Zhang, D.-X. Wang, H.-W. Ma, Q.-Y. Zheng and M.-X. Wang, *Chem. – Eur. J.*, 2006, **12**, 9262–9275.
43 M.-h. Yang, T.-W. Lin, C.-C. Chou, H.-C. Lee, H.-C. Chang, G.-H. Lee, M.-k. Leung and S.-M. Peng, *Chem. Commun.*, 1997, 2279–2280.
44 C.-C. Wang, W.-C. Lo, C.-C. Chou, G.-H. Lee, J.-M. Chen and S.-M. Peng, *Inorg. Chem.*, 1998, **37**, 4059–4065.
45 C.-Y. Yeh, C.-H. Chou, K.-C. Pan, C.-C. Wang, G.-H. Lee, Y. O. Su and S.-M. Peng, *J. Chem. Soc., Dalton Trans.*, 2002, 2670–2677.
46 K.-Y. Ho, W.-Y. Yu, K.-K. Cheung and C.-M. Che, *J. Chem. Soc., Dalton Trans.*, 1999, 1581–1586.
47 J. L. Bolliger and C. M. Frech, *Tetrahedron*, 2009, **65**, 1180–1187.
48 J. L. Bolliger, M. Oberholzer and C. M. Frech, *Adv. Synth. Catal.*, 2011, **353**, 945–954.
49 S. Narayan, T. Seelhammer and R. E. Gawley, *Tetrahedron Lett.*, 2004, **45**, 757–759.
50 Y.-J. Cherng, *Tetrahedron*, 2002, **58**, 887–890.
51 J. F. Hartwig, in *Handbook of Organopalladium Chemistry for Organic Synthesis*, ed. E.-I. Negishi and A. de Meijere, John Wiley & Sons, New York, 2002, vol. 1, pp. 1051–1096.
52 R. J. Lundgren, A. Sappong-Kumankumah and M. Stradiotto, *Chem. – Eur. J.*, 2010, **16**, 1983–1991.
53 M.-k. Leung, A. B. Mandal, C.-C. Wang, G.-H. Lee, S.-M. Peng, H.-L. Cheng, G.-R. Her, I. Chao, H.-F. Lu, Y.-C. Sun, M.-Y. Shiao and P.-T. Chou, *J. Am. Chem. Soc.*, 2002, **124**, 4287–4297.
54 R. H. Ismayilov, W.-Z. Wang, G.-H. Lee and S.-M. Peng, *Dalton Trans.*, 2006, 478–491.
55 S.-A. Hua, I. P.-C. Liu, H. Hasanov, G.-C. Huang, R. H. Ismayilov, C.-L. Chiu, C.-Y. Yeh, G.-H. Lee and S.-M. Peng, *Dalton Trans.*, 2010, **39**, 3890–3896.
56 J. F. Berry, F. A. Cotton, P. Lei, T. Lu and C. A. Murillo, *Inorg. Chem.*, 2003, **42**, 3534–3539.
57 C.-J. Wang, H.-R. Ma, Y.-Y. Wang, P. Liu, L.-J. Zhou, Q.-Z. Shi and S.-M. Peng, *Cryst. Growth Des.*, 2007, **7**, 1811–1817.
58 C.-X. Yin, J. Su, F.-J. Huo, R.-H. Ismayilov, W.-Z. Wang, G.-H. Lee, C.-Y. Yeh and S.-M. Peng, *J. Coord. Chem.*, 2009, **62**, 2974–2982.

59 W.-C. Hung, M. Sigrist, S.-A. Hua, L.-C. Wu, T.-J. Liu, B.-Y. Jin, G.-H. Lee and S.-M. Peng, *Chem. Commun.*, 2016, **52**, 12380–12382.
60 P. Stanetty, J. Röhrling, M. Schnürch and M. D. Mihovilovic, *Tetrahedron*, 2006, **62**, 2380–2387.
61 D. Blomberg, K. Brickmann and J. Kihlberg, *Tetrahedron*, 2006, **62**, 10937–10944.
62 M. Castillo, P. Forns, M. Erra, M. Mir, M. López, M. Maldonado, A. Orellana, C. Carreño, I. Ramis, M. Miralpeix and B. Vidal, *Bioorg. Med. Chem. Lett.*, 2012, **22**, 5419–5423.
63 K.-i. Seki, K. Ohkura, M. Terashima and Y. Kanaoka, *Heterocycles*, 1994, **37**, 993–996.
64 E.-X. Zhang, D.-X. Wang, Q.-Y. Zheng and M.-X. Wang, *Org. Lett.*, 2008, **10**, 2565–2568.
65 N. H. Werstiuk and C. Ju, *Can. J. Chem.*, 1989, **67**, 5–10.
66 B. Yao, D.-X. Wang, H.-Y. Gong, Z.-T. Huang and M.-X. Wang, *J. Org. Chem.*, 2009, **74**, 5361–5368.
67 M.-J. Huang, S.-A. Hua, M.-D. Fu, G.-C. Huang, C. Yin, C.-H. Ko, C.-K. Kuo, C.-H. Hsu, G.-H. Lee, K.-Y. Ho, C.-H. Wang, Y.-W. Yang, I.-C. Chen, S.-M. Peng and C.-h. Chen, *Chem. – Eur. J.*, 2014, **20**, 4526–4531.
68 F. A. Cotton, L. M. Daniels, C. A. Murillo, I. Pascual and H.-C. Zhou, *J. Am. Chem. Soc.*, 1999, **121**, 6856–6861.
69 A.-L. Barra, F. Bianchi, A. Caneschi, A. Cornia, D. Gatteschi, L. Gorini, L. Gregoli, M. Maffini, F. Parenti, R. Sessoli, L. Sorace and A. M. Talarico, *Eur. J. Inorg. Chem.*, 2007, 4145–4152.
70 J. Sandström, *Dynamic NMR Spectroscopy*, Academic Press, London, 1982.